JOURNAL OF GEOPHYSICAL RESEARCH, VOL. 93, NO. B5, PAGES 4182-4198, MAY 10, 1988

A NUMERICAL MODEL FOR THE MECHANICAL BEHAVIOR OF INTRAPLATE VOLCANOES

Luc Chevallier and Wilhelm J. Verwoerd

Department of Geology, University of Stellenbosch, South Africa

Abstract. A new approach toward understanding the mechanical behavior of intraplate volcanoes is offered by first postulating a geological model of the internal structure and then developing an axisymmetric numerical simulation using the finite element method. This enables one to consider the types of fracturing at various depths in terms of state of stress under specific conditions of loading. The geological model is based on comparative field studies of three volcanically active oceanic islands (Marion, Tristan da Cunha, and Rèunion) and a dormant one (Gough). The model contains a shallow (3 km deep) magma chamber with distinguishable floor, wall, and roof sections. A magma column rises from the chamber toward a central cone at the surface. Depending on the structural level at which they originate, different dyke and fracture patterns are generated. For the numerical simulation the medium is assumed to be linear elastic, continuous, and isotropic. Different loading combinations are applied, including hydrostatic pressure plus magmatic pressure in the chamber and external pressure that represents regional tectonic effects. It appears that the structural levels of the geological model can be adequately explained by variations in the distribution, intensity, and trajectories of principal stresses σ_1, σ_2, and σ_3. It is concluded that the shape of the magma source is a major factor in the stress pattern. The effect of the driving pressure ($P_{mag} - P_{ext}$) on the orientation of the principal stresses σ_1 and σ_2 is also considered. The sloped surface of the volcanic edifice is found to cause local rotation of the stress field. Finally, the evolution of the stress field with loading path is related to successive structural levels in a dynamic eruptive model.

Introduction

Pressurized magma in a reservoir or in a planar fissure is the main source of stress and strain inside a volcanic edifice. Variation of the geometrical and physical characteristics of this source determines the distribution and intensity of the stress and displacement fields. The general problem that needs to be solved in modeling volcanoes is to determine what connections exist between (1) surface observations, (2) stress and displacement fields, and (3) the characteristics of the source. In other words, what can be learned about the source (shape, size, depth, pressure) through mechanical analysis, knowing volcanic surface phenomena? This is known as an inverse problem.

The approach in this paper is twofold. First, a geological model is established that idealizes the internal structure of an intraplate volcano. Second, this model is tested from a mechanical point of view.

The geological model is based on a comparative study of several volcanic edifices. Therefore the model does not represent the simplified picture of a specific volcano but rather a theoretical synthesis of all the features that have been observed on different volcanoes: tectonics, structure, morphology and eruptive dynamics.

The mechanical analysis was done by numerical simulation using the finite element method. It will be shown (see section below on the physical and elastic properties of the model) that the assumption of a linear elastic and continuous medium is quite justified in this case. We are mainly interested in the distribution and intensity of stresses, since they give the most probable sites where fractures are going to open, keeping in mind that the medium is continuous. The subject matter of this paper therefore belongs to the first category of problems discussed in the historical review below.

Finally, in the discussion, the geological and numerical models are compared.

Paper number 7B7030.
0148-0227/88/007B-7030$05.00

Historical Development of Mechanical Modeling in Volcanology

Previous work on the mechanical behavior of volcanoes uses both analytical and numerical methods, and can be subdivided into three categories. The first category of problems is the distribution of stresses inside a volcanic edifice. Mechanical models of the internal structure of volcanoes started with Anderson's [1935] studies on the origin of the cone sheets and ring dykes of Ardnamurchan in Scotland. By an analytical approach, he derived the equations of displacement components due to a radial point dilatation and a vertical point-push acting in a weightless, semi-infinite, elastic, isotropic half-space. He concluded that cone sheets occupy tensile fractures while ring dykes occupy shear fractures (Figure 1a). Jeffreys [1936] criticized Anderson's assumption that the complete form of the fracture can be directly inferred from the distribution of stress before fracture. In fact, the form of the fracture depends both on the original stress field and on the changes introduced as the fracture develops. In this regard, Robson and Barr's [1964] approach that compared the distribution of stresses with the strength of the rock is certainly more realistic and arrived at quite contrary conclusions to those of Anderson. Their analytical method used the stress function for an infinite solid in which an infinitely long horizontal cylindrical hole is contained. These stress equations were calculated for a deviatoric field with P_{max} vertical (lithostatic pressure), P_{min} horizontal (regional pressure), and P_{int} in the cylinder (hydrostatic). Combining these equations with the Coulomb-Navier criterion for shear failure, they developed critical parameters at which shear failure or tensile failure will occur (Figure 1b). According to this model, cone sheets are likely to develop along planes of shear dipping inward, whereas centrally intruded dykes propagate along vertical tensile cracks. Another of their conclusions is that shear failure occurs only when the magma body is at a sufficient depth of 4.7 km. In his dynamical approach, Phillips [1974] supported the idea of cone sheets forming along shear failure planes.

The second category of problems deals with the propagation of cracks. To model such cracks, Pollard [1973a] derived the equations of stress and displacement around a pressurized elliptical hole in a homogeneous isotropic solid. He showed [Pollard, 1973b] that large principal stress differences and large stress gradients are concentrated at the termination of the crack (Figure 1c). He defined propagation mechanisms (extension, ductile, brittle) propagation criteria (the magma pressure must only slightly

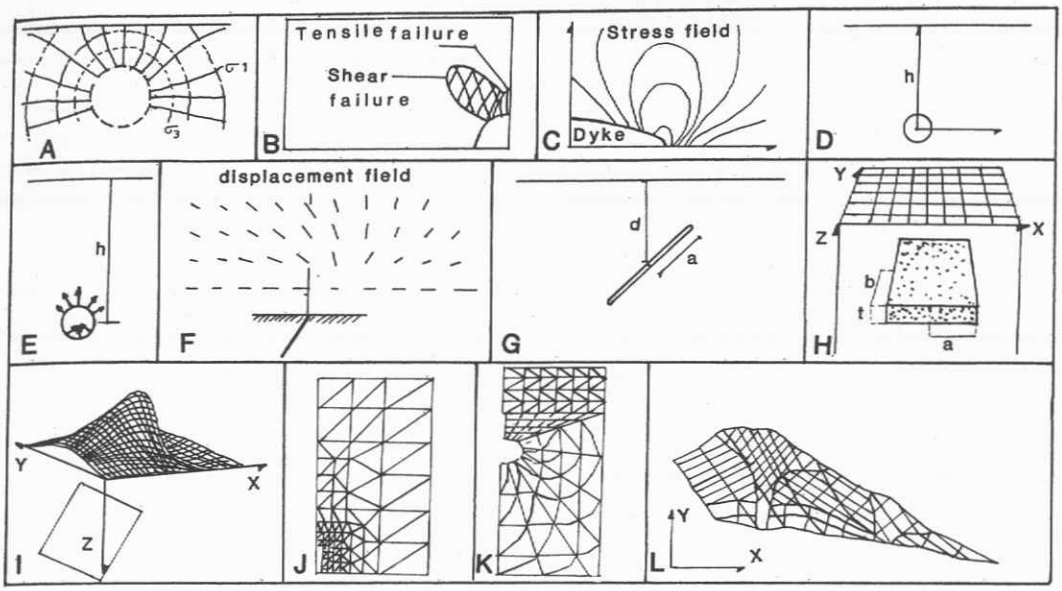

Fig. 1 Historical development of mechanical modeling of volcanoes (see text for explanation). (a) Anderson [1935], (b) Robson and Barr [1964], (c) Pollard [1973b], (d) Mogi [1958], (e) Yokoyama [1971], (f) Walsh and Decker [1971], (g) Pollard and Holzhausen [1979], (h) Ryan et al. [1983], (i) Davis [1983], (j) Dieterich and Decker [1975], (k) Bianchi et al. [1984] and (l) Paul et al. [1987].

exceed the regional stress normal to the length of the fissure), and factors that influence propagation direction like the orientation of the regional stress. The influence of the regional stress field on dyke orientation has also been modeled by Tsunakawa [1983] and documented with geological examples by Nakamura [1977] and Muller [1986]. The latter author reconstructed, with a finite element model, the paleodirection of the regional stress field components during emplacement of the Spanish Peaks dykes.

The third category of problems relates ground deformation on active volcanoes to the deformation field produced by idealized sources of pressure and displacement. Such models date from the work of Mogi [1958], who used the expression for horizontal and vertical displacements caused by the change of hydrostatic pressure in a small sphere (depth of burial much larger than the dimension of the cavity) in a semi-infinite elastic solid, and from these obtained the surface deformation (Figure 1d). He estimated the depth of the chamber for Kilauea and Sakurajima volcanoes. His method, which is very simple because only one parameter is necessary (the depth of burial), has been widely used [Eaton, 1962; Fiske and Kinoshita, 1969; Jackson et al., 1975]. Nevertheless the simplicity of the model (geometry of the source, pressure distribution, and characteristics of the medium) is often the cause of departures between computed and observed deformation and an overestimation of the depth of burial. The model developed by Yokoyama [1971] is an alternative to Mogi's assumption, having a variable pressure distribution on the wall of the sphere (Figure 1e). The results obtained are similar to those of Mogi's model.

Walsh and Decker [1971] developed a more realistic model. Vertical and horizontal displacements and tilt at the surface are derived for a dipping line source (a pipe) extending to depth. The model employs an elastic, isotropic half-space, and the approach is analytic (Figure 1f). Application of this model to Kilauea shows that the theoretical field for a vertical source at 1.5 km compares favorably with displacements observed during different periods of activity. However, different parameters (length, intensity, dip) can give the same displacement field, so the model lacks uniqueness. Pollard and Holzhausen [1979] used a fluid-filled fracture (Figure 1g). The problem is more complex and needs the superposition of two analytical solutions. Interesting conclusions have been drawn, such as the difference of concentration of stress at both tips of the slit and the strong asymmetry of the displacement field when the slit is near the surface. Pollard et al. [1983] proposed this model as a solution to estimate the geometric and physical parameters of dykes intruded in volcanic rift zones. Their analytical approach, which also considers stress, enables the authors to associate the distribution of open cracks on the surface with the state of stress developed by the dyke. This model has been used with success by Bonazia et al. [1984] to interpret ground deformation at the Phlegrean Fields. In addition, the stresses are roughly consistent with the observed seismicity of 1983.

The model developed by Ryan et al. [1983] represents an original approach. It gives the three-dimensional deformation field generated by the withdrawal of magma from a sill-like storage compartment (Figure 1h). The method is semi-analytic, i.e., it combines a general analytic solution for displacement components with a point-by-point space step computational approach. The medium is considered anisotropic with different elastic parameters for vertical and horizontal directions. The model has been applied to deformation and eruptive events at Kilauea volcano. Quantification of the location, dimensions, and orientation of the sill-like magma body is then combined with a three-dimensional model of Kilauea's internal structure deduced from earthquake hypocenters. The model of Davis [1983] is also three-dimensional but completely analytic. The displacement field is produced by a dipping rectangular dislocation with fluid pressure, in a uniform elastic half-space (Figure 1i). The method effectively determines dip and orientation followed by depth, length, height, and width in order of increasing uncertainty. The model has not been applied to a volcano but provided a convenient starting point for the interpretation of ground deformation. Good fit is obtained with the two-dimensional analysis by Pollard and Holzhausen [1979] in Figure 1f.

Dieterich and Decker [1975] were the first to use the finite element method, allowing them to test a wider range of shapes and depths for a buried magma body in an isotropic, elastic half-space (Figure 1j). Application to Kilauea volcano is illustrated by two examples:

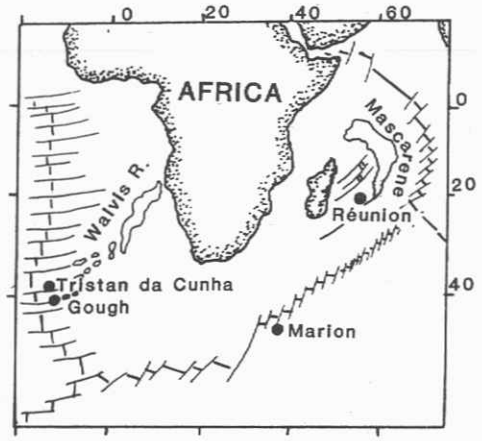

Fig. 2 The four intraplate volcanic islands selected for comparative study.

axisymmetric analysis for summit deformation and plane strain analysis for East Rift Zone intrusions. For the period of inflation between January and February 1967, a vertical cigar-shaped conduit at 0.7 km depth is in best agreement with the surface deformation. Modeling of the East Rift Zone intrusions has suggested the presence of southward dipping sheets. More recently, Bianchi et al. [1984] developed a finite element model for ground deformation observed at the Phlegrean Fields. The magmatic system is composed of an oblate-spheroid chamber (the volume of which is derived from thermal analysis) and a vertical intrusion (Figure 1k). The originality of the model is to consider temperature dependent elastic parameters that change the properties of the medium. The results are in good agreement with the large and rapid uplifts experienced by the Phlegrean Fields. Finally, a numerical model called "Bloc" has been used by Paul et al. [1987] and applied to the landslide of Mount St. Helens in 1980. The model Bloc, derived by the finite element method, is adapted for the behavior of anisotropic and fractured media composed of the juxtaposition of blocks with three degrees of freedom: two translations and one rotation (Figure 1l). Linear elastic, nonlinear elastic, or elastoplastic media can be modeled. For the failure of the flank of Mount St. Helens the best fit between the observed and the computed surface displacements is obtained for a coefficient of friction of 0.5 and additional earthquake simulation. However, this is not a unique solution because the same results are obtained in the case of a dipping intrusion or a sloped substratum. In the case of Mount St. Helens, the geology permits the choice of the second solution.

This historical review covers a period of 50 years of research during which some 25 papers have been published. Despite the fact that this list is probably not exhaustive and that all these contributions represent important steps in the mechanical modeling of volcanoes, studies in this domain are definitely less numerous than in other fields of volcanology. Two major problems remain: (1) uncertainties are often due to nonuniqueness of the solutions in inverse problems, and (2) very often there is a lack of geological constraints even though the modeling technique itself may be improved. Both problems are in fact linked, since geology can be used to elucidate uncertainties. The contribution of this paper is more geologic and therefore differs from the above.

Comparative Geological Study

Four intraplate volcanoes have been chosen for comparison to establish the geological model: Marion Island and Piton de la Fournaise (on Rèunion) in the Indian Ocean, Tristan da Cunha and Gough in the South Atlantic Ocean (Figure 2). Marion, Piton de la Fournaise, and Tristan da Cunha are active, whereas Gough is dormant. They all display alkaline or transitional to alkaline geochemical trends.

Marion Island

Marion and its neighbor Prince Edward Island are located 300 km south of the southwest Indian axial rift. Both volcanoes lie on an aseismic submarine plateau adjacent to a $N20^0E$ striking fracture zone (Figure 3a). This $N20^0E$ structure as well as the E-W trend of the ridge are reflected in the morphology of the plateau and on both volcanoes (cliffs, dykes, faults) and caused the collapse of four fifths of the Prince Edward edifice. The volcanism of these islands therefore appears to be controlled by regional tectonics, and reactivation of paleostructures has been proposed as an alternative solution to the fixed mantle plume hypothesis to explain their origin [Chevallier, 1986]. The fact that both islands displayed the same rhythm of activity during the past (based on stratigraphic and geochronologic comparisons [Verwoerd, 1971; McDougall, 1971a] points toward the role of regional tectonic movements along the same fracture zone of the seafloor. However, reactivation of such structures is expected to take place on a geological time scale. Off-ridge seismic activity has been recorded only once on the $N20^0E$ fracture zone and never on the Marion submarine plateau, since the world seismic network started in 1958.

Marion is a shield volcano with slopes that do not exceed 8^0 (Figure 3c). Like its neighbor, Prince Edward, it has been built up during the Pleistocene and Holocene periods and is characterized by strombolian eruptions located along well-developed radial faults [Verwoerd, 1971; McDougall, 1971a]. The magma is an alkaline basalt with a trend of differentiation to trachybasalt. The most recent eruption took place in 1980 [Verwoerd et al., 1981] and is the only one recorded since the discovery of the island in 17[illegible] although some flows appear to be fresh.

Structural analysis [Chevallier, 1986], stratigraphic and petrologic studies (work in progress) reveal the presence of two volcanic centers (Figure 3b). The east center corresponds to the building of the main shield. The west center grew later on the flanks of the former, developing a short but well-developed rift zone trending NE-SW. Both centers were active simultaneously at least during the Holocene period. This double structure is reflected in the morphology by the "bean" shape of the island. The Santa Rosa Valley, in which very few eruptions occurred, is interpreted as a huge landslide generated by repeated intrusions along the arcuate rift zone.

Volcanism on Marion is chiefly marked by strombolian activity with scoria cones between 40 and 200 m high and lave flows of aa type; pahoehoe is subordinate. The strombolian vents have a large average spacing of 1.5 km and are located along radial faults delimiting low-lying areas. These lowlands, although less pronounced than the Santa Rosa Valley, have also been interpreted as landslides as a result of general instability of the flanks of the volcano. Following the studies by Fedotov [1976] and Wood [1980] on the relation between the size of cinder cones and depth of magma chambers, a depth greater than 3 km has been proposed for the magma source under Marion [Chevallier, 1986]. Hawaiian activity is less common. It is characterized by en èchelon segmented fissures marked by spatter ramparts or small scoria cones. Finally, surtseyan activity occurred on the submerged coastal plain, producing bedded hyaloclastic tuff cones [Verwoerd and Chevallier, 198[illegible]. The rate of activity on Marion is very low. A mean of one eruption per century can be estimated for the Holocene period (15,000 years). The other outstanding feature

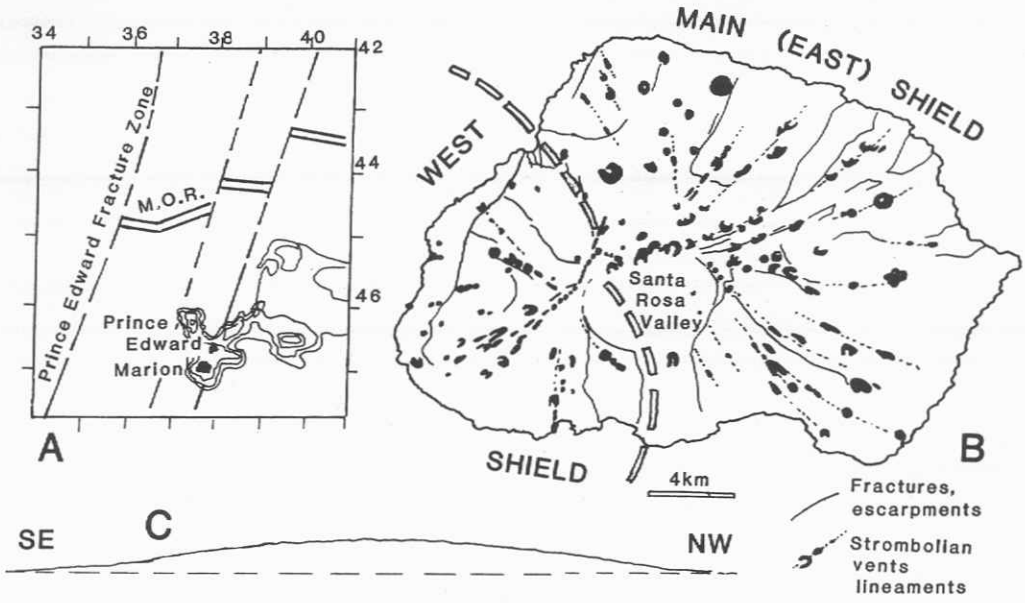

Fig. 3 Marion volcano. (a) Regional tectonic setting (b) Structural sketch map of Marion. The West shield developed later on the flank of the main (East) shield. (c) Profile of Marion as seen from Prince Edward. Note the absence of a central cone.

Marion volcano is the absence of pronounced central activity and summit calderas at both centers. The eruptive activity can be described as typically radial and equally distributed on the flanks of the two shields.

The principal characteristics of Marion volcano are summarized in Table 1.

Gough Island

Gough Island is located 500 km east of the South Atlantic axial rift. It lies on a fracture zone of the seafloor also marked by two other seamounts, McNish and RSA, immediately ENE of Gough (Figure 2). The magma extruded constitutes an alkaline suite:
Gough basalt, trachybasalt, trachyandesite, and trachyte [LeMaitre, 1960, 1962]. The volcano was built up during the Pleistocene (1 Ma), and the last eruption of Edinburgh Peak is dated at 0.13 Ma [LeRoex, 1985].

Recent structural studies [Chevallier, 1987] have led to a distinction between two phases of construction: a basaltic phase closed by a caldera collapse, and a trachytic phase. The basaltic volcano is characterized by a curved elongated shape that continues below sea level (Figure 4a). Gough Island has been deeply eroded by radial valleys and by the sea, so that the original morphology of the volcano is no longer preserved. However, the radial natural cross sections show a profile with a clear steepening of the slope toward the center (Figure 4b). This leads to the conclusion that a well-developed central cone existed before the caldera collapse and erosion took place.

The basaltic series was fed and intruded by a dense radial dyke system converging toward the center of the edifice where Edinburgh Peak eventually became the site of the latest eruption on the island. A N125^{0}E parallel dyke swarm is a prominent component of this system and corresponds to the elongation of the island. In this intrusive zone the dyke/country rock ratio is 40%. It narrows toward the center of the volcano, where the dyke density increases to nearly 100%. It has been interpreted as a denuded volcanic rift zone. The rest of the radial system is composed of swarms in which the density of intrusion is 20% on average, becoming progressively more dense toward the center of the edifice. The type of basaltic activity on Gough is unfortunately difficult to document. Thick flows, aa flows, and interstratified scoria cones are found. The density of the intrusive system and the rarity of big scoria cones suggest that fissure eruptions rather than strombolian eruptions may have occurred toward the center.

At the end of the basaltic period a caldera was formed. It corresponds to the Tarn Moss plateau, which shows a morphology typical of infilling. The term "shield caldera" has been given to this collapse. A shield caldera is defined

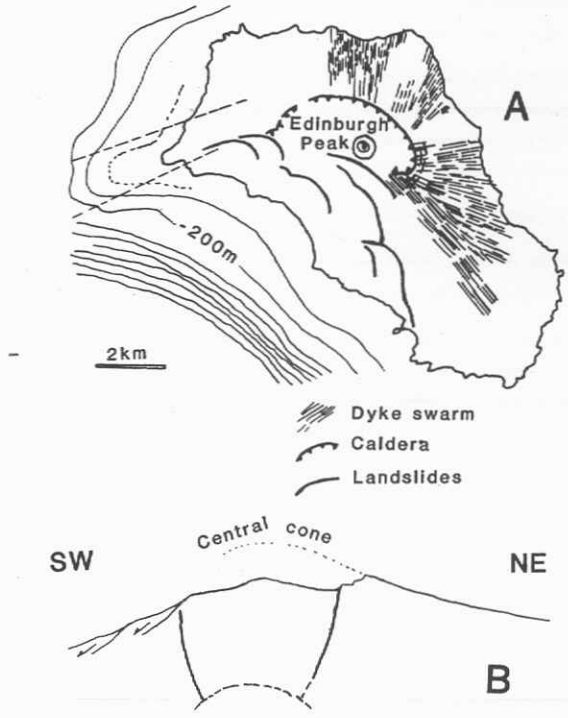

Fig. 4 Gough volcano. (a) Structural map. (b) Cross section. The existence of a central cone during the basaltic period is inferred from the paleoprofile of the edifice.

as one that has a large diameter relative to the diameter of the edifice and heralds the close of a magmatic period. On the other hand, a summit caldera (for which we have no firm evidence on Gough because of erosion but which does exist elsewhere, e.g., on Piton de la Fournaise; see below) has a small diameter compared with the diameter of the edifice and is contemporaneous with the volcanic activity. From the size of the caldera on Gough, a 4-km-deep magma chamber has been inferred. It is possible that this caldera may have been initiated by cone fracturing, as suggested by concentric dykes (cone sheets?) that intruded along its rim.

A SW-NE profile of the island shows the strong asymmetry of the volcano. On the southwest the caldera was open to the sea (where most of the trachytic flows escaped). Slope breaks affecting the basaltic substratum and the general arcuate morphology of the edifice suggest that landslides, similar to that of Santa Rosa Valley on Marion, developed on the flanks during the basaltic period.

The trachytic volcanism produced plugs, domes, thick flows, and thin pumice fall deposits. It is not detailed in this paper, since the comparison will be restricted to basaltic edifices in order to arrive at a model of a basaltic volcano.

A summary of the main features of this volcano is given in Table 1.

Tristan da Cunha

The Tristan group comprises three islands: the active volcano of Tristan da Cunha and the two eroded older edifices, Inaccessible and Nightingale, all three resting on the same submarine plateau. This is located on the edge of the South Atlantic Ridge, 500 km east of the axial rift. It is the westernmost volcanic pile of a group of scattered seamounts, forming the western portion of the Walvis Ridge.

The comprehensive petrological account by Baker et al. [1964] shows that the volcanic rocks belong to a potassic alkaline suite: k-alkali basalt, k-trachybasalt, k-trachyandesite, k-trachyte. The trachybasalt is by far the most abundant lava. McDougall and Ollier [1982] published apparent K-Ar ages ranging from 0.21±0.01 to 0.01±0.02 Ma, and Ollier [1984] gave a geomorphological description of the three islands.

Recent geological investigations led to a new dynamic interpretation of the volcano [Chevallier and Verwoerd, 1987]. Volcanic activity on Tristan da Cunha appears to be characterized by a dual feeding system: central and lateral (Figure 5a). This duality is first reflected in the morphology of the edifice that clearly shows a steep (30^0) central cone and low-angle (8^0) lateral flanks. Second, the distribution of dykes and cones strengthens the conclusion. A dyke swarm is well exposed in the central cone because of strong erosion. The density of intrusion, which is far higher than in the cliffs surrounding the island, as well as their excellent radial pattern centered on the summit, are good arguments to conclude that the dykes exploited hydraulic fractures generated by a magma column (Figure 5b). The lack of fissure activity on the flanks of the central cone suggests that none, or few, of these dykes could have been eruption feeders and that the central activity appears to be restricted to a summit position, i.e., at the top of the magma column. Abundant pyroclastic products have been ejected through the summit crater as a result of hydrovolcanic activity due to the presence of a lake and/or a shallow water table. This pyroclastic material contributed in large part to the construction of the central cone.

In contrast, the lateral activity occurred at a much lower level on the flanks of the volcano. The style of eruption was strombolian, resulting in scoria cones and flows. Dykes and a number of lateral vents occurred along radial fractures that appear to be concentrated along two tectonic axes trending $N170^0E$ and $N80^0E$ (Figure 5a). These directions

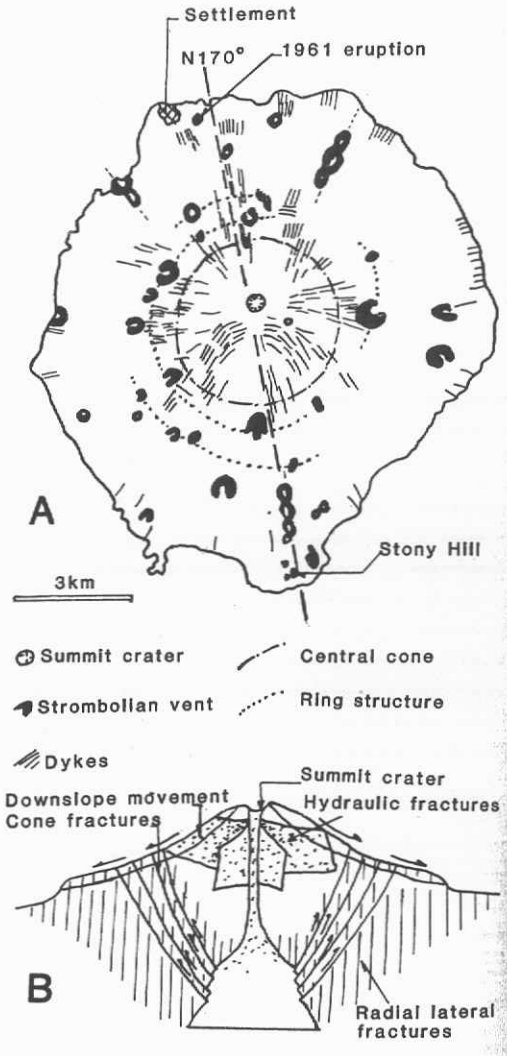

Fig. 5. Tristan da Cunha volcano. (a) Structural map. The $N170^0E$ tectonic axis is parallel to the compressive component of the regional stress field. (b) Internal structure of the edifice inferred from surface observations.

are also found in the morphology of the underwater edifice as revealed by marine bathymetry. Axis $N170^0E$ is recognized as the major one for several reasons: (1) it corresponds to long dykes and eruptive fissures, (2) it connects the two most recent eruptions (1961 and Stony Hill) of rather unusual character (trachyandesitic, entirely effusive), and (3) it is the direction of a slight migration of the summit crater. This tectonic axis is also parallel to the compressive component of the stress field recorded for a cluster of earthquakes in the seafloor 500 km north of the island. As in the case of Nakamura's [1977] examples Spanish Peaks [Muller, 1986] and the Canary Islands [Fera et al., 1985], it is concluded that the regional stress field has played a role in the orientation of the dykes of Tristan da Cunha.

A concentration of vents in a circular zone around the central cone leads to the conclusion that the effect of a ring structure is added to the radial fracturing. Conical fracturing is inferred at depth. Accepting the dynamic interpretation of Phillips [1974] for cone sheet emplacement, such cone fractures on Tristan da Cunha probably result from shear planes created by uplift of the roof of the magma chamber (Figure 5b). In this case the uplift must have contributed to the elevation of the central con-

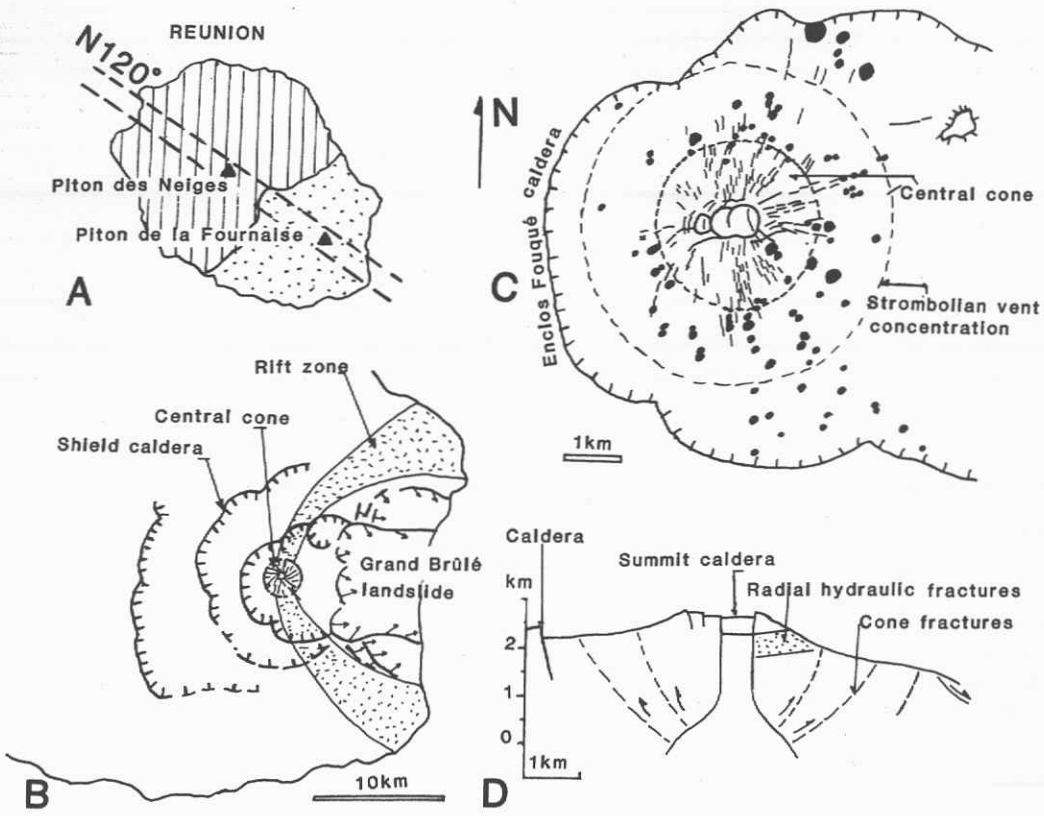

Fig. 6 Piton de la Fournaise volcano. (a) A N120?E structure guided the evolution of Réunion Island and is parallel to an abandoned portion of the Mid-Indian Ocean Ridge (Figure 2). (b) General structural map of Piton de la Fournaise. (c) Detail of the most active central part of the volcano. (d) Cross section and inferred internal structure.

Considering the diameter of the ring structure, a magma chamber not deeper than 5 km can be inferred for Tristan da Cunha volcano.

Finally, segmented en èchelon fissures can be seen in plan, and segmented en èchelon dykes have been observed in vertical cliffs as they approach the surface and feed scoria cones [Chevallier and Verwoerd, 1987]. They are related to slope instability; similar conditions also exist at other volcanoes. If a dyke propagates to the surface, it will enter a zone of mixed mode stress, i.e., tensile separation plus antiplane shearing, as a result of topographic contributions to the three-dimensional stress field, and will start segmenting. However, on Tristan da Cunha, slope failures or landslides did not develop as on some other volcanoes (Marion, Gough, Piton de la Fournaise), where supplementary triggering factors, e.g., a volcanic rift zone, exist.

The characteristics of Tristan da Cunha volcano are summarized in Table 1.

Piton de la Fournaise on Rèunion

The Mascarene Archipelago is composed of the three volcanic islands of Rèunion, Mauritius, and Rodriguez (Figure 2). Rèunion Island consists of two overlapping shield volcanoes. The older one is the dormant Piton des Neiges, Pleistocene in age [McDougall, 1971b]. Its final eruptive phase has been dated at 0.03 Ma [Gillot and Nativel, 1982]. The younger one is the active volcano of Piton de la Fournaise built on the southwest flank of the former at 0.36 Ma [McDougall, 1971b] (Figure 6a). Relationships between magnetic anomalies and transform faults on the one hand and the structure and tectonics of Rèunion and Mauritius on the other hand suggest that the volcanism of the Mascarene Islands has been structurally controlled and that the Rèunion volcanoes resulted from reactivation of a paleorift N120^{0}E dated by magnetic anomaly 27 [Chevallier and Vatin Perignon, 1982]. Piton des Neiges and Piton de la Fournaise were built up on this N120^{0}E direction (Figure 6a).

Piton de la Fournaise lavas consist of transitional slightly alkaline basalt [Upton and Wadsworth, 1972; Ludden, 1978]. Structural studies [Chevallier and Bachélery, 1981; Bachélery and Chevallier, 1982] show that the volcano evolved over four periods, each characterized by specific structures, tectonics, and magmatic evolution. The first three periods are concluded by three large caldera collapses (Figure 6b), which are inferred to be connected with deep subcrustal magma chambers. The edifice has a horseshoe structure as a result of arcuate volcanic rift zones and a huge landslide (the Grand Brûlé) affecting its east flank, so that the caldera is open to the sea. This landslide has been interpreted as resulting from the combined effect of a sloped substratum (the Piton des Neiges) and the emplacement of dykes along the curved rift zones. Activity along the rift zones outside the caldera is rather weak (six eruptions recorded in 300 years) but is characterized by big strombolian vents and great volumes of lava.

Ninety five percent of the present activity is restricted to the caldera of Enclos Fouqué (Figure 6c). The activity is fairly central and is concentrated around a 600-m cone with 25^0 slopes (Figure 6d). The rate of activity is high, with an average of one eruption every 1.5 years, but the magma discharge is low: 0.32 m^3/s, compared with 0.8 m^3/s on

Etna and between 1 and 3 m^3/s on Hawaii [Bachélery, 1981]. A series of pit craters (or summit calderas) occupy the summit of the cone. They consist of overlapping circular cauldrons. Their rapid evolution (succession of opening, enlarging, and infilling) has been recorded since the eighteenth century and is inferred to reflect the migration of an axial magma column within the cone. This column develops a dense system of radial hydraulic cracks that feed eruptions on the flanks of the central cone. These eruptions are chiefly of the fissural type, with spatter cones and spatter ramparts, and are emplaced along en échelon segments that migrate from top to base, and usually last from a few hours to a few days. Accurate mapping and structural analysis of the summit area allowed the demarcation of zones of extension and sliding on the central cone [Bachélery et al., 1982]. General instability toward the east and the southeast is found and controls the tectonic pattern of eruptions.

On the lower flanks of the cone and on the floor of the caldera, eruptions are more strombolian in style, building small scoria cones (20 to 50 m high) and are steady for a few days to a few weeks, producing a greater amount of lava than the central eruptions. As on Tristan da Cunha, a concentration of strombolian vents around the base of the central cone suggests the presence of conical fracturing at depth. The central cone owes its origin both to accumulation of short lava flows and to uplifting as a result of shearing along these conical fractures.

Since 1980 a volcanological observatory has monitored the volcano. Earthquakes recorded before eruptions indicate a shallow magma chamber (between 2 and 4 km) below the summit [Bachélery et al., 1982; Lenat et al., 1988].

Table 1 provides a summary of the principal characteristics of Piton de la Fournaise volcano.

The Geological Model

The many features that these four examples have in common (Table 1) allow the construction of a combined geological model of an ideal intraplate volcano.

First, it has been shown above that regional tectonics makes an imprint on oceanic intraplate volcanoes in two ways: (1) by reactivation of preexisting structures and (2) by local response to the regional stress field. Marion and Réunion islands exhibit good evidence of reactivation. This kind of tectonics affects the whole lithosphere, regulating the volcanism on a geological time scale, but does not influence the geometry of the feeding and eruptive systems in the upper parts of the edifice and at the surface. Such tectonics is a long-range phenomenon which will not be taken into account in our mechanical model. On the other hand, the stress field developed inside a volcano, due to regional pressures, can be of great importance in this study. Nakamura's [1977] assumption that beyond the influence of the magma chamber, dyke intrusion would occur in parallel with the maximum compressive regional stress, has been confirmed by mechanical modeling on theoretical grounds [Tsunakawa, 1983] and on geological grounds in the case of Spanish Peaks, Colorado [Muller, 1986]. Parallelism between the direction of principal regional stress deduced from dyke orientations and recorded compressive movement has been established on volcanoes of the Canary Island group in the North Atlantic [Ferraud et al., 1985]. Similarly, we have related the main direction of intrusion on Tristan da Cunha with the direction of compression recorded in the seafloor 500 km north of the island [Chevallier and Verwoerd, 1987]. Unfortunately, such relationships cannot be established for the other islands. The regional stress field is still a great unknown in most oceanic areas. Nevertheless the influence of a regional stress field can be simulated by horizontal side pressure on a mechanical model as shown below.

An idealized geological model of the internal structure of an intraplate volcano is given in Figure 7. Deep volcanic roots connected to production zones or subcrustal magma chambers are not detailed, since too little documentation exists at this stage. Only Piton de la Fournaise displays a series of wide caldera rims that may bear a direct relationship with deep and wide magma chambers. The upper structural levels are better known and have been used in this model.

The Magma Chamber

In all four examples, tectonics, structure, and eruptive dynamics point toward a shallow reservoir between 2 and 4 km below the summit. An average depth of 3 km for the shallow reservoir has been found on many other basaltic volcanoes, e.g., Kilauea [Decker, 1987; Klein et al., 1987] and Krafla in Iceland [Tryggvason, 1986; G. Sigvaldason, oral communication, 1987]. This depth corresponds as well to a state of mechanical equilibrium, or "neutral buoyancy" [Ryan, 1987b] inside volcanoes.

The shape and size of this reservoir are based on the geometry of plutonic complexes that can be found around the world and are supposed to represent ancient magma chambers. The plutons of the Kerguelen Archipelago [Giret, 1983; Giret and Lameyre, 1983] are of special interest here. First, they were undoubtedly once connected to oceanic intraplate volcanoes of the Indian Ocean, like those described in this paper. Second, they have an age range of 23 m.y., thus reflecting different structural levels exposed by different degrees of erosion: deep, hypovolcanic, and subvolcanic. The deep complexes are characterized by stratified peridotite and gabbro, like the ophiolites, attributable to magmatic sedimentation on the flat bottom of a chamber. The hypovolcanic complexes of Kerguelen display a half-ovoid shape with successive cooling envelopes from basic on the outside toward more differentiated inside. They range between 1 and 10 km in diameter, averaging about 4 km. The shallower, subvolcanic complexes are not relevant to our model: they are connected with more siliceous differentiates, plugs, and plutonic bodies less than 1 km in diameter. Other examples of gabbroic to granitic complexes that may be interpreted as cooled magma reservoirs within shield volcanoes occur in southeastern Iceland, e.g., the Vesturhorn intrusion, 3 km wide [Roobol, 1974]. It thus seems reasonable to postulate an idealized magma chamber 3 km deep and 3 km wide, with a flat floor and sloping wall and roof sections. The flat floor has been chosen arbitrarily in order to take into account the effects of magmatic sedimentation encountered in many complexes. The break between the roof and the wall is also arbitrary. It is there to be mechanically tested as a possible explanation for the formation of cone fractures.

The Magma Column

Central activity is observed on Piton de la Fournaise, Tristan da Cunha, and Gough and is ascribed to the rise of a magma column above the chamber. Such a magma column explains the summit eruptions, the central cone, the radial system of dykes or eruptive fissures, and the summit caldera or craters observed on the three volcanoes cited above. Although the summit caldera may be temporarily occupied by a lava lake, the column never extends to the surface but is plugged by the sunken block; this causes a reentrant angle in the idealized model. It is considered that at any time the column will be partly molten and partly consolidated.

TABLE 1. Summary of the Comparative Geology Between the Four Studied Volcanoes

Marion	Gough	Tristan da Cunha	Piton de la Fournaise
Regional structural control on the volcanism.	---	Regional stress field influence on the structure of the volcano.	Regional structural control on the volcanism.
Two magma reservoirs inferred at a depth > 3 Km	An inferred 4 Km-deep magma chamber.	A magma chamber that cannot be deeper than 5 km.	A two-fold magmatic system: a deep subcrustal chamber connected to large calderas and a shallow reservoir (3 km) feeding eruptions.
Shieldlike profile, no central cone.	A central cone, much eroded.	A very well developed central cone resulting from accumulation and uplift.	A well-developed central cone.
---	Central activity attested by a high concentration of dykes near the center.	A magma column rising above the chamber and important summit activity.	A column rising above the shallow reservoir and a summit caldera above the column.
Weak radial fissure activity	Dense central dyke network.	Central radial dykes	A radial central system of fissure eruptions.
Typical strombolian lateral activity along pronounced radial fractures.	Lateral radial activity also well developed.	Radial lateral dykes with strombolian lateral activity.	Lateral fractures with weak strombolian activity.
An arcuate rift zone.	A prominent linear rift zone but arcuate structure of the volcano.	---	An arcuate rift zone.
No caldera or pit crater.	A shield caldera with a few cone sheets.	Cone fractures in depth responsible for ring structure and uplifting of the central cone.	Cone fractures in depth responsible for ring structure and uplifting of the central cone.
Large-scale land-sliding connected with the rift zone.	Huge landslides connected with the rift zone.	Downslope movements on the flanks.	Downslope movements on the central cone and huge landslides on the lower flank due to arcuate rift zone and sloped substratum.
Low production rate.	Production rate unknown.	Production rate unknown.	High production rate.

The Summit Caldera

At the top of the magma column a summit caldera or pit crater may form. Piton de la Fournaise shows one, whereas Gough is too deeply eroded. Summit calderas are ephemeral structures that evolve rapidly as a function of the magma supply, the discharge rate, the migration of the column, and stability of the collapsing block. In the case of Tristan da Cunha, a summit crater is present but resulted from explosive, hydrovolcanic activity.

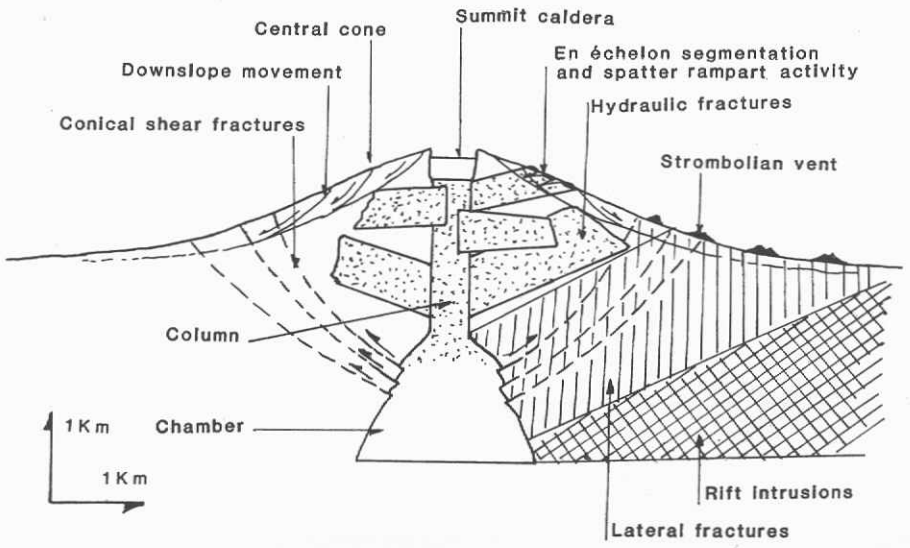

Fig. 7 The geological model and different structural levels.

The Radial Hydraulic Fractures

The column develops a dense system of radial hydraulic fractures responsible for the fissure eruptions described on the surface. Hydraulic fracturing can occur when the pressurized magma (that acts as the fluid in this case) is injected into the discontinuities of the country rock and opens them up. A radial hydraulic fracture will form when the magma pressure is higher than the combined magnitude of the tangential component of the least compressive stress (σ_3) and the tensile strength of the rock. Such conditions can be met easily within the central cone.

The Lateral Fractures

Lateral activity, responsible for strombolian eruptions, is very prominent on Gough and Marion but less prominent on Tristan da Cunha and Piton de la Fournaise. We suggest that the lateral vents are fed by dykes generated at a deeper level than the central radial fractures, i.e., on the walls of the magma chamber itself. Due to higher confining pressure, tension cracks are likely to occur. Tension cracks develop under a high deviatoric stress field and high magnitude of the principal compressive stress σ_1. Crack propagation is parallel to the direction of this stress. This, as many other aspects of the model, will be tested in the numerical simulation. Hydraulic fracturing will facilitate the propagation of the fissure if the conditions, explained above, are satisfied.

The Cone Fractures

Adopting Phillips' [1974] dynamical model, cone sheets (or fractures) form as a result of uplifting of the roof of the magma chamber, resulting in an uplift of the central part of the volcano. This is most likely to happen if the profile of the chamber has a break between wall and roof as shown in Figure 7. The cone fractures represent shear planes along a zone of weakness as shown in Robson and Barr's [1964] model. This does not necessarily mean that cone sheets will form, resulting in a well-defined ring structure at the surface, but will favor the concentration of lateral eruptions around the base of the central cone, as illustrated by Tristan da Cunha and Piton de la Fournaise. The Gough caldera, formed during the close of the basaltic period, may also be related to such a cone fracture system. On Marion, a caldera is not evident.

The Rift Intrusions

Rift eruptions are thought to form as a result of large withdrawals of magma from the bottom portion of the chamber. This assumption will have to be tested from the mechanical point of view.

The Central Cone

A well-developed central cone is present on two volcanoes (Tristan da Cunha and Piton de la Fournaise) and is inferred on Gough, but does not exist on Marion. This goes together with the fact that Marion is a volcano without characteristic central activity. The central cone has a dual origin: (1) accumulation of pyroclastic and effusive products as a result of prominent central activity and (2) uplift associated with shear cone fractures at depth. An average slope of 25^0 is assumed in our model.

Downslope Movements

On the flanks of the volcanic edifice, downslope movements of two kinds are common. In the first kind, the topographic effect develops a mixed mode stress field in the superficial parts of the edifice. The en échelon segmentation of dykes has been attributed to the presence of this near-surface stress field [Chevallier and Verwoerd, 1987]. In the second kind a full landslide develops. Triggering factors are necessary in this case, e.g., dyke emplacement along an arcuate volcanic rift zone (Marion, Gough, Piton de la Fournaise). For Piton de la Fournaise the sloped substratum formed by the Piton des Neiges volcano would be an additional factor. The same kind of relationship between landslide, curved intrusive zone, and sloped substratum is described on Kilauea [Duffield, 1975; Swanson et al., 1976; Lipman et al., 1985] or Mauna Loa [Lipman, 1980]. However, Gough and Marion show that a sloped substratum is not essential but the arcuate intrusive zone is.

Our geological model thus based on a comparison of a few islands represents an average oceanic volcano. All examples show some degree of correspondence or departure from this general model. The next question is: what stress distribution is to be expected in the model, and how can the divergences be understood in terms of mechanical behavior and source characteristics?

The Numerical Model

Description

The analysis of the displacement and stress field utilized is a direct application of the finite element method which is treated in detail by Cheung and Yeo [1979]. The basis of the finite element method is that the medium to be analyzed is approximated by an assembly of structural elements joined at their nodal points. The displacement components at these nodes become the unknowns of the problem when external forces are applied to the structure. These displacements are determined by the following systems of equations:

$$F = K\,U$$

where F is a matrix that lists the external forces, U is a matrix of resulting displacements, and K is a stiffness matrix of the structure. K is obtained by summing the stiffness matrices for each element which are a function of their shape, nodal point coordinates, and elastic constants in linear problems. Complex computer programs exist for solving such problems in engineering. The one that we used at the Institute for Structural Engineering of the University of Stellenbosch is called ABAQUS and uses quadrangular elements.

As shown in Figure 8, the idealized geometry used for the numerical simulation is based on the geological model. It represents a volcano with its central cone and more gentle lower flanks, resting on a piece of oceanic crust. The lateral extent of the crust has been arbitrarily chosen so as to give sufficient distance from the magma system. The magma system is composed of a chamber (floor, walls, roof) and a column. The model is axisymmetric, i.e., it represents a slice of a volcano that can be repeated around the vertical axis. Displacements and stresses in the plane of the section can be calculated. Tangential stresses, perpendicular to the plane can also be calculated, but the tangential displacements are zero. The mesh layout was determined by the areas where additional accuracy was needed.

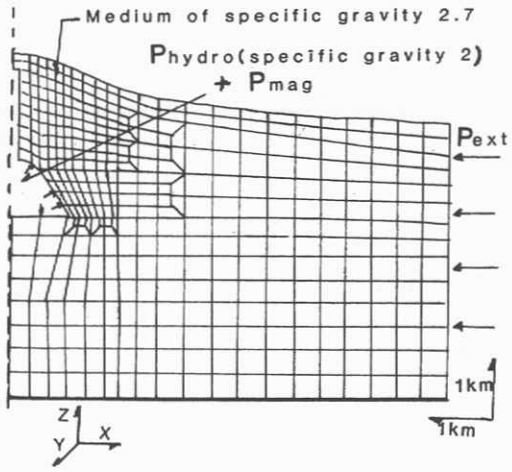

Fig. 8 Mesh layout of an axisymmetric numerical model. Thick line (bottom) delimits a constrained boundary where only horizontal displacement in the X direction is allowed. The dashed line delimits the axis of symmetry along which only vertical displacement in the Z direction is allowed. The thinner boundary line (surface, side, magma system) has no constraints. See text for other explanations and the loading of the model.

Boundary Conditions

At the bottom of the crust the vertical displacement in the Z axis direction is equal to zero. The horizontal displacement in the X axis direction is free.

Along the axis of symmetry of the model, the horizontal displacement in the X axis direction is equal to zero. The displacement in the vertical direction (Z axis) is free.

The topographic surface, the lateral limit of the crust, and the boundary of the magma system are free. Vertical (Z axis) and horizontal (X axis) displacements are allowed.

Physical and Elastic Properties of the Model

The medium (i.e., the basalt of the oceanic crust and the volcano itself) is assumed to be continuous, and this can be justified by the large scale of the object being modeled. Indeed the degree of fracturing at this scale is such that the material can be considered as continuous. The same approximation is currently accepted in soil mechanics and gives satisfactory results. It must be said that at smaller scales this approximation will not be true.

It is also assumed that the medium follows a linear elastic law. This is acceptable if the limitations of such a model are made explicit. We are interested in the distribution and intensity of stresses around the magma body and not in the opening and propagation of cracks that need criteria of failure and the use of an elastoplastic law. Our approach that combines geological observations and linear elastic mechanical analysis, can be seen as an alternative to a purely mechanical elastoplastic approach.

Finally, the medium is taken to be isotropic (or homogeneous), i.e., it possesses the same elastic properties everywhere. This last approximation is certainly not entirely justified, especially as far as temperature is concerned. The elastic parameters will change from the hot chamber to the cold surface. Models are presently being computed that will allow this factor to be taken into account. The elastic parameters are the Young modulus E=75,000 MPa and the Rigidity modulus G=30,000 MPa (Poisson ratio V=2.5). These values are for an average basalt at ambient temperature [Carmichael, 1982; Clark, 1986]. Ryan [1987a] provides curves of the elastic properties of Hawaiian basalt as a function of temperature. This recently published work could not be taken into account in our study, but the parameters obtained by the author for low temperatures (E=60,500 MPa and G=26,100 MPa) are the same order of magnitude as those used here.

The Load Cases

The body forces (the weight) are applied vertically to each element of the model based on a specific gravity of 2.7 assigned to the medium. The body forces are responsible for the resulting vertical and horizontal lithostatic pressures. They take the place of the linearly increasing confining pressure on horizontal model sections as the depth increases.

The hydrostatic pressure exercised by the magma as a fluid of specific gravity 2 is represented by a force applied at each element face of the boundary of the magma system, and perpendicular to the surface of each element concerned. The choice of a density of 2 for the molten magma is arbitrary and serves only to give a difference of buoyancy between the magma and the country rock.

Magmatic pressure (due to gas expansion and magmatic confinement) is an overpressure compared with an initial stage where hydrostatic pressure and gravity are in equilibrium. To explain the surface displacements, a magnitude of 35 MPa for magmatic pressure has been used in the models of Dieterich and Decker [1975] and Bianchi et al. [1984]. Paul et al. [1987] use magmatic pressure up to 90

MPa to explain the surface displacement of Mount St. Helens. In our model, magmatic pressure (P_{mag}) up to 55 MPa has been applied, in addition to the hydrostatic pressure, at every element face of the magma system boundary, perpendicularly to the element face concerned.

Deformation in the crust in general occurs for very low values of the differential horizontal pressure (between 1 and 10 MPa). This is proven by in situ measurements [Paquin et al., 1984] and by mechanical analysis [Cloetingh and Wortel, 1985]. Regional pressure is here considered to be an external force due to a remote stress field and is constant with depth, i.e., it is related to intraplate movements (modeled in this case as pure shear). This force has been applied at every node of the vertical side of the model (P_{ext}). It is independent of the horizontal component of the lithostatic pressure which, as discussed above, enters as a body force.

The aim of our model is to look at the resulting stress field that will be in static equilibrium with all these different loads: (1) the weight, (2) the hydrostatic pressure of the magma, (3) the magmatic pressure itself due to gas expansion, and (4) the external pressure due to the remote stress field.

The Loading Path

The numerical model was initialized solely with the overburden weight. This loading case is not totally realistic and is not detailed below, but it does permit us to control the effect of the lithostatic pressure (vertical and horizontal). This first step also acts as a reference, rather than the undistorted shape, to calculate the vertical and horizontal displacements in the medium. Such data will be relevant to a study of ground deformation, which is outside the scope of this paper.

In the second step, hydrostatic pressure is applied in the magma chamber and in the column.

Finally, different pressure combinations (P_{mag}/P_{ext}) are applied to the model. Pressure intensities were chosen not for their absolute value, which has no great meaning in linear elastic problems, but to give different deviatoric stress, i.e., driving pressure values ($P_{ext} - P_{mag}$). Nevertheless their order of magnitude must be realistic to compete with the action of hydrostatic pressure and gravity. The following results are described in the sequence of increasing driving pressure and increasing magmatic pressure (from 0, i.e., hydrostatic pressure only, to 55 MPa in "combined" pressure).

Stress Distribution and Intensity

Among numerous data sets obtained from the numerical analysis, four characteristic loading combinations show increasing values for the driving pressure (5, 15, 30, and 50 MPa) and are presented here (Figure 9). Principal stresses $_1$ and σ_2 occur in the cross-sectional plane of the model, andσ_3 is thus normal to it.

The principal stress σ_1 is everywhere compressive (negative numbers). It results chiefly from the action of lithostatic pressure and increases strongly with magmatic pressure. It is mainly concentrated on the wall and on the floor of the chamber, where its intensity reaches a maxmimum. Along the upper third of the column it is a weak function of depth and is little affected by magmatic pressure. A concentration of stress is also noticed at the top of the column even when hydrostatic pressure alone acts in the chamber. This solution was expected, considering the geometry assumed for the model, and it is supposed to simulate the weight of the summit caldera block on top of the magma column.

Away from the magma reservoir the principal stressσ_2 is compressive and increases with depth as expected (see Figure 10). This monotonous stress field is strongly perturbed around the magma system, where it is alternatively compressive and tensile at different depths (Figure 9). It is compressive at the base of the column, on the wall, and the floor of the chamber. Compressive stresses remain fairly constant as magma pressure increases. Tensile stresses are connected with sharp corners like the top of the column and the bottom corner of the chamber, where its intensity rapidly increases with magmatic pressure. At the roof of the chamber the stress is zero to slightly tensile and becomes slightly compressive to zero away from the boundary of the chamber.

The principal stress σ_3 is tangential to the magmatic system and is perpendicular to the section plane (by definition in an axisymmetric model). In the crust, σ_3 is compressive and it increases with depth. Around the magma system, the field where the stress is tensile is quite large: along the column, on the roof, and in the bottom corner of the chamber. When hydrostatic pressure acts alone in the chamber, the highest tensile tangential stress is concentrated at the base of the column. As the magmatic pressure increases, the envelope of stresses progressively becomes parallel to the column. In the bottom corner of the chamber the tensile stress remains constant. Along the profile of the chamber, tensile stress σ_3 decreases as compressive stress σ_1 increases. The point where the tangential stress becomes compressive corresponds to the maximum of compressive stress σ_1.

Stress trajectories

Only σ_1 and σ_2 trajectories can be in the plane of the section (Figure 10). Stress σ_3 is thus perpendicular to the plane, and it acts horizontally.

The driving pressure (P_{mag}-P_{ext}) has an effect on the trajectories of the compressive principal stress, σ_1 (Figure 10). When only hydrostatic pressure acts in the chamber, the trajectory is mainly guided by the lithostatic pressure. As the deviatoric field increases, the trajectories on the wall of the chamber are reoriented toward the periphery of the edifice. The influence of external pressure is especially marked in comparison of Figures 10b and 10c. The addition of P_{ext} to the side of the model induces a strong reorientation of the compressive principal stress, σ_1, at the bottom corner of the magma chamber.

Along the column, the compressive principal stress is horizontal, even when hydrostatic pressure is acting alone. At the base of the column its trajectory is oblique and directed toward the surface. The driving pressure has no effect on the orientation of the stress.

The gravity effect of the sloped surface is revealed in the stress pattern. Principal compressive stress (σ_1) undergoes a rotation, particularly striking in the central cone, and becomes subparallel to the surface. In the case of low deviatoric field, i.e., when P_{ext} is large compared with P_{mag}, the zone concerned with this rotation is thicker (Figures 10b and 10c).

Principal stress σ_2 is sometimes tensile with a very restricted distribution. It corresponds to concentrations of stress at sharp corners of the magma system profile.

Discussion

The aim of this study is not to predict from numerical simulation alone where and how fractures will open and propagate, but rather to compare a geological model, based on observed volcanological features, with the corresponding computed stress field.

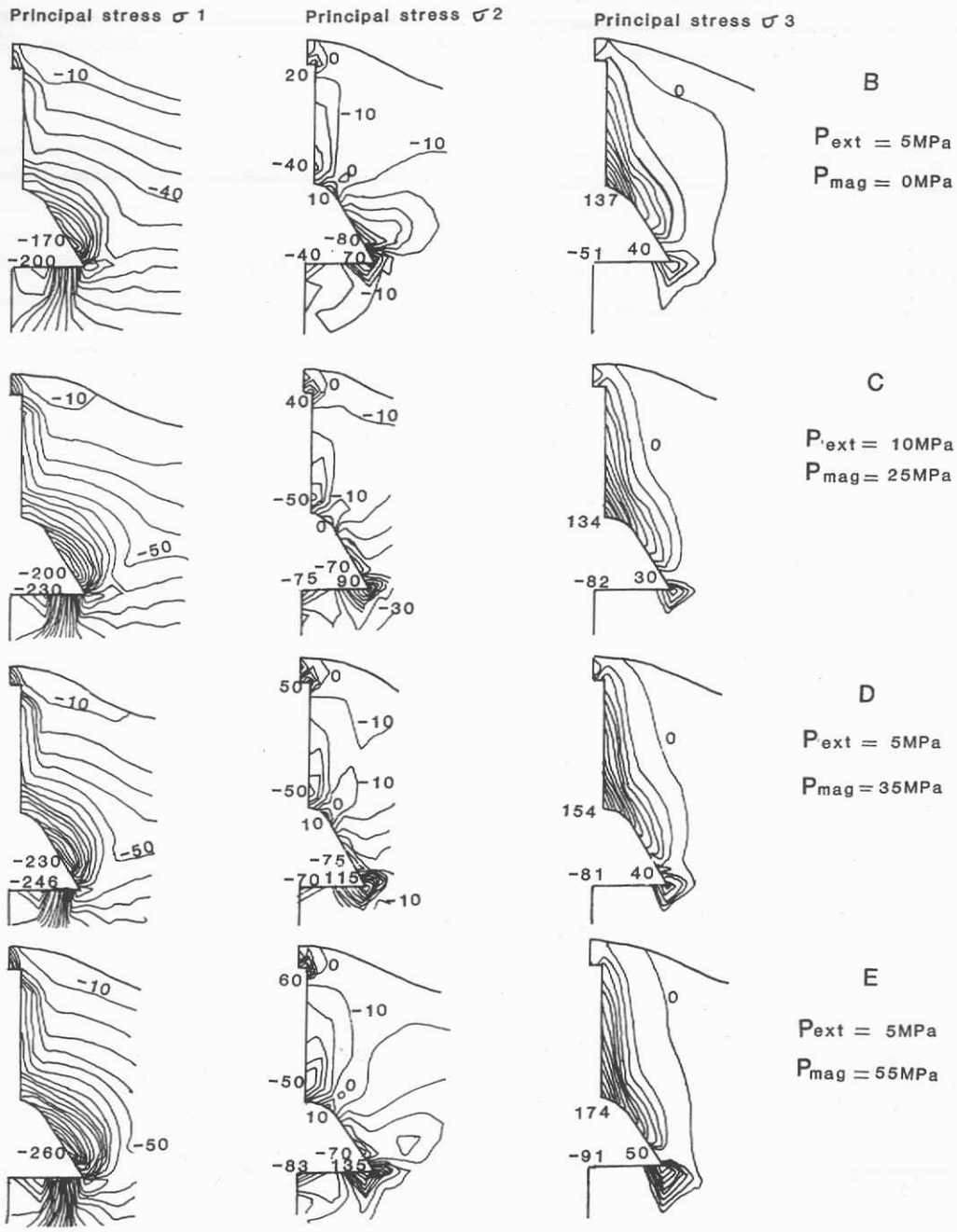

Fig. 9 Principal stress distribution and intensity. Load combinations are annotated B, C, D, and E to correspond with the load combinations of Figure 10. Contours at 10-MPa intervals. Negative values indicate compression, and positive values indicate tensile stress. For each case, the body forces and hydrostatic pressure have been applied.

Internal Structure and Stress Field

A coherent stress pattern can be associated with each structural level of the geological model (Figure 11). At the top corner of the column, stresses σ_2 and σ_3 are tensile but σ_3 remains constant whereas σ_2 is greater and increases with magmatic pressure. This is a coherent stress distribution for such a geometry. Mechanical conditions are in good agreement with conical fractures delimiting a summit caldera. However, pit craters generally have a more cylindrical shape. An elastoplastic analysis of a discontinuous medium would be essential for the study of the mechanics of such sinking blocks.

Alongside the column, stresses σ_1 and σ_2 are compressive, and stress σ_1 is horizontal. They remain fairly constant when magmatic pressure increases (compared with the other parts of the magma system), whereas tensile stress σ_3 increases. The corresponding structure generated is that of a dense swarm of radial hydraulic fractures. From the mechanical point of view, the intrusion of pressurized magma into such a fracture will be helped by the increasing tensile stress σ_3 and will only have to exceed the tensile strength of the rock, which is small along discontinuities. Conditions will be satisfied for hydraulic fracturing to occur, but propagation of the fracture cannot be predicted by an elastic continuous model. At the base of the column

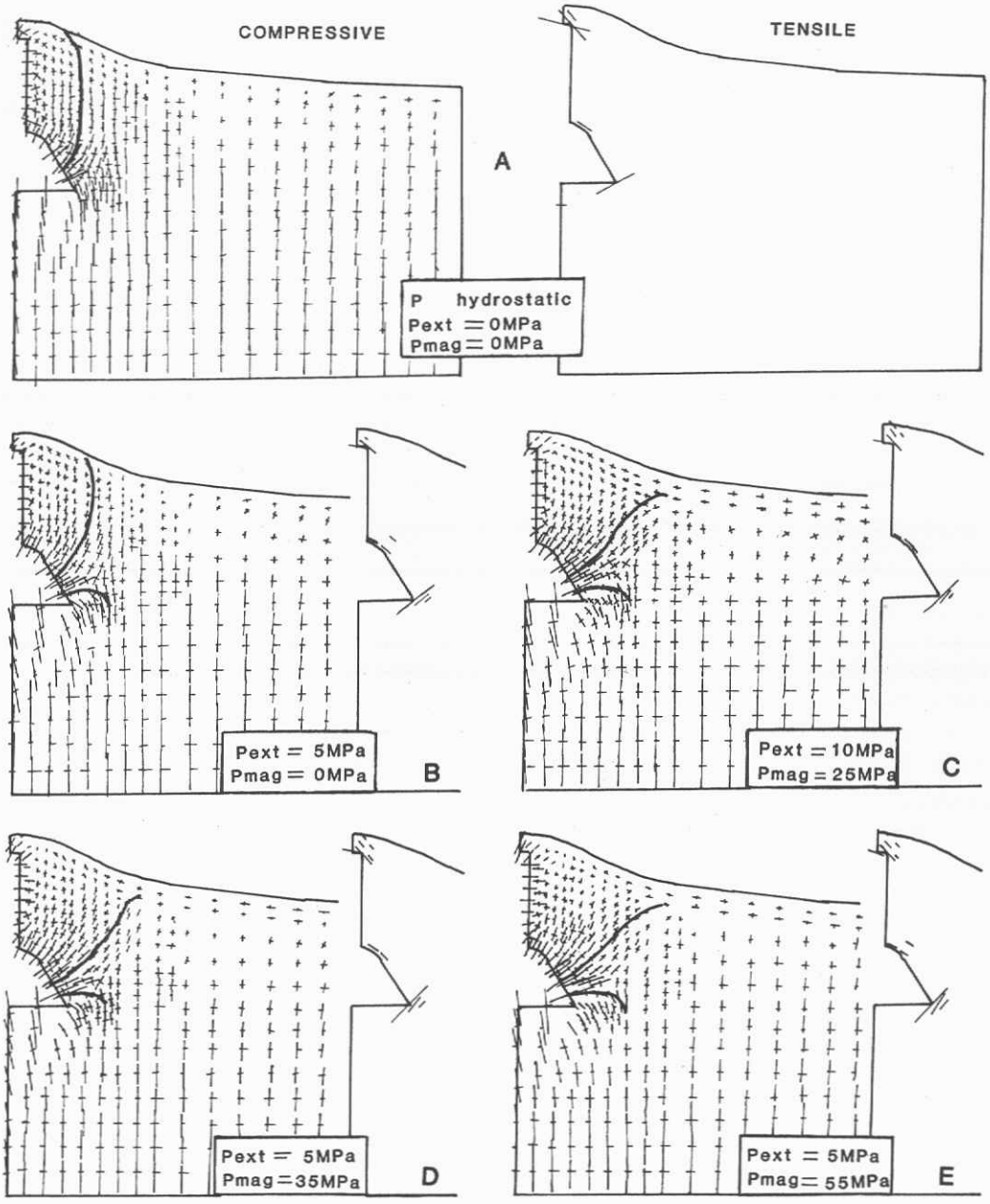

Fig. 10 Trajectories of principal stresses σ_1 (direction of the long axis of the cross) and σ_2 (short axis of the cross). The magnitude of stress is proportional to the length of the cross axes. Principal stress σ_3 is tangential to the axis of symmetry and is horizontal and perpendicular to the plane of the section; therefore it cannot be shown. Hydrostatic pressure and body foces are present in every case. For each loading case, two figures are shown, one displaying the trajectories of the compressive stresses (σ_1 and σ_2) and the other the trajectories of the tensile stresses (only σ_2).

the situation is comparable to the above except that compressive stresses σ_1 and σ_2 rotate and become oblique to the boundary.

At the transitional zone between the roof and the wall of the chamber the principal compressive stress σ_1 increases with magmatic pressure. Stress σ_2 is tensile to zero, and σ_3 is tensile. According to the geological model, this is the zone where the lateral strombolian radial eruptions and conical shear fractures originate. The stress pattern helps to elucidate this phenomenon. Since stress σ_3 is tensile, the feeding fracture will be radial. On the other hand, the large difference between compressive stress σ_1 and stress σ_2 (the latter being zero or slightly compressive away from the boundary) will favor the formation of conical compressive shear fractures in response to the growing magnitude of τ_{xy}. Nevertheless, it must be kept in mind that shearing also depends to a large extent on other rock mechanical parameters such as coefficients of friction and cohesion.

On the wall of the chamber, stress σ_1 is compressive, very large, and increases strongly with magmatic pressure. The tangential stress σ_3 is slightly tensile. It follows that the dykes feeding lateral eruptions can be interpreted as tension cracks. This means that the trajectory of such fractures would be largely fixed by conditions obtained before fracturing. It was shown above that this trajectory is guided by the value of the driving pressure ($P_{mag}-P_{ext}$).

At the bottom corner of the chamber, stresses σ_2 and σ_3 are tensile and the compressive stress σ_1 becomes horizontal

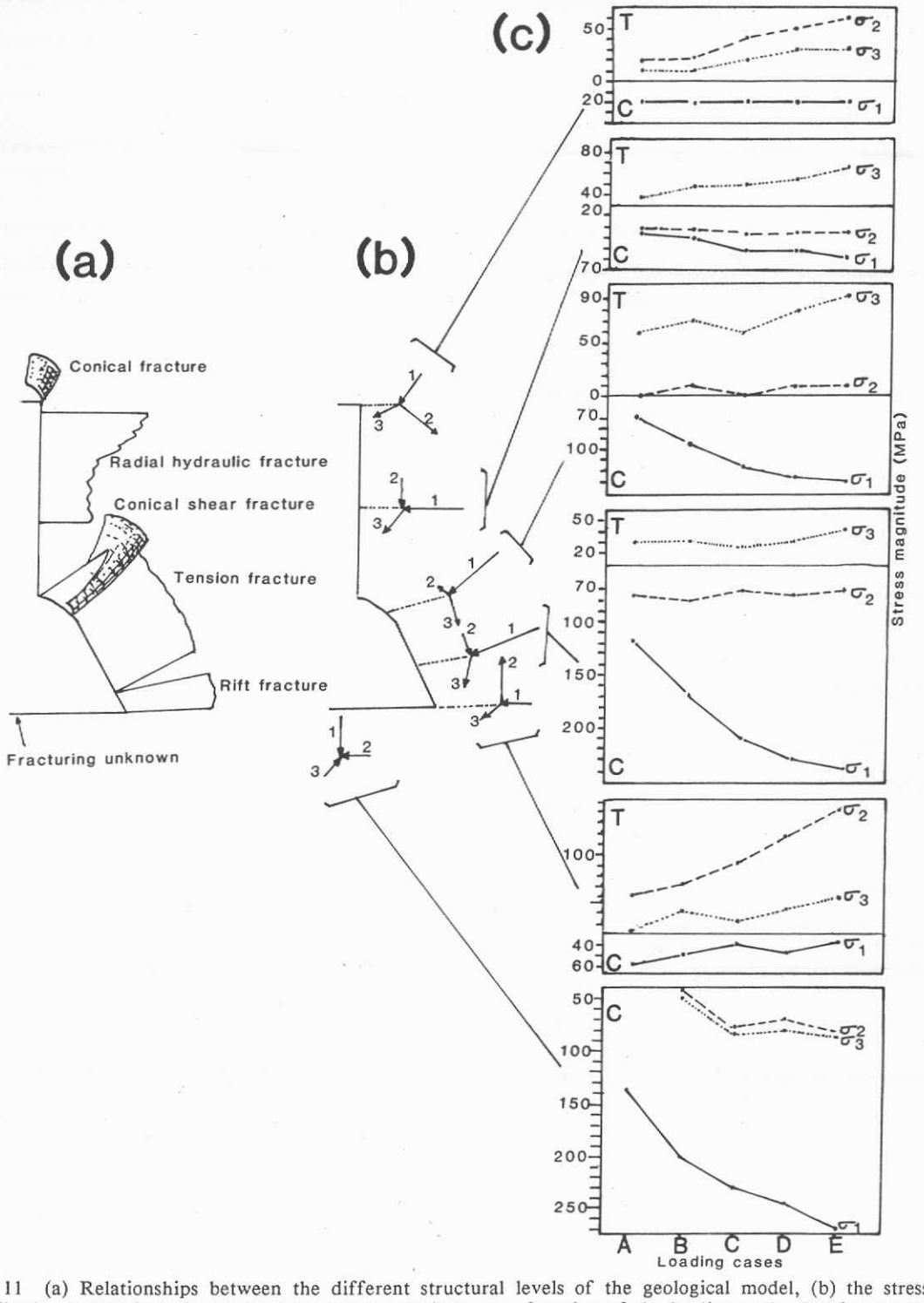

Fig. 11 (a) Relationships between the different structural levels of the geological model, (b) the stress distribution and trajectories, and (c) the stress magnitude as a function of the loading path. In Figure 11b σ_1, σ_2 are in the plane of the section and σ_3 is shown in perspective, with the average stress magnitude indicated by the length of the arrow. The loading cases (A,B,C,D,E) are those used in Figure 10. T stands for tensile, and C for compressive stress.

when P_{ext} is added to the load case. In the geological model, that is where rift eruptions would be generated. As a point of fact, the high magnitude of tensile stress σ_2 would result in a widening and enlargement of the corner of the chamber by the creation of sill-like fractures and intensive withdrawal of magma from the reservoir. On the floor of the chamber the stresses are all compressive. Simple shear or pure shear would be expected, but no geological observations have been made on this structural level.

Eruptive Scenario

It is interesting to see how the stress field evolves with the loading path (i.e., increasing magma pressure slightly

modified by external pressure) and what structural levels are successively involved (Figure 11c).

Along the column the profiles of stresses σ_1, σ_2, and σ_3 remain fairly flat. At the beginning of the loading path a stress field close to isotropic conditions and low in magnitude prevails between σ_1 and σ_2. On the roof and on the wall of the chamber the profiles of the stresses have the same shape and therefore react similarly to the pressure changes. They are characterized by a quick increase of stress σ_1 when P_{ext} and then P_{mag} are added to hydrostatic pressure and an asymptotic flattening of the curve for high pressure. A large deviatoric stress field exists between σ_1 and σ_3 when high pressure is applied. On the botton corner, tensile stress σ_2 increases rapidly and compressive stress σ_1 remains constant.

Among the four volcanoes reviewed in this paper, only Piton de la Fournaise has a sustained activity. It is well documented for the last 50 years, and the volcano has been monitored by an observatory since 1980; five eruptions have occurred since then. Seventy percent of the eruptive cycles follow a similar pattern [Kieffer et al., 1977; Krafft and Gérente, 1977a, b; Chevallier et al., 1981; Bachélery et al., 1982; Lénat et al., 1988]. They usually start at the top of the cone or high on its flanks with the opening of short-lived radial cracks, and then migrate down the flanks to become steady at a lower level. Very few eruptions evolve along the rifts, but when they do so, a great amount of magma is produced. In this scenario the different structural levels of the magmatic complex are successively activated: (1) column, (2) roof and wall, (3) bottom of the chamber. This may be compared with the loading path (Figure 11). In the first steps of increasing pressure (load cases A, B, C), stress fields σ_1 and σ_2 are constant, very low, and isotropic along the column. The value for stress σ_3 is relatively high. Hydraulic radial cracks are easily generated but cannot last long because of pressure building up in the deeper structural levels. As the magmatic pressure increases (second step, cases C, D, E), compressive stress σ_1 reaches its maximum on the roof and the wall of the chamber. Lateral tension cracks will form at this stage, their direction being guided by the driving pressure. Finally, if the magmatic pressure still increases (beyond E), stress σ_2 will continue to increase, and widening will occur at the bottom of the chamber from where rift eruption will be generated. Delimitation between the different eruptive zones and the different loading steps cannot be sharp and will necessarily overlap. It is difficult at this stage to test this eruptive scenario at Marion or Tristan da Cunha, the main reason being the lack of sustained activity and detailed chronology.

It must be realized that this parallelism between eruptive scenario, internal structural levels, and loading path is still very rough. Most active volcanoes exhibit many variations in the detailed sequence of eruptive events. These variations can probably be assigned to differences and changes in geometric parameters of the magma chamber and the physical characteristics of the medium. Furthermore a loading path on an elastoplastic discontinuous medium would give different mechanical behavior.

Conclusion

The approach adopted here is original in the sense that it establishes relationships between different internal structural levels of a volcano inferred from multiple geological observations, and a stress field computed by numerical simulation. In a way it can be seen as a continuation of Anderson's [1935] work.

This idealized basaltic volcano, comprising a magma chamber with a roof and walls and a column rising above it, is certainly not a unique model, but it permits an explanation of several of the internal and surface volcanic features in terms of behavior under stress. Departures are found, like the lack of typical central activity on Marion, with its attendant radial hydraulic fracture system, the lack of a conical structure and a well-developed lateral system instead. A poorly developed magma column and a small magma chamber without a break in the profile may provide an explanation on this case.

The shape of the chamber certainly plays the major role in the distribution of stress inside a volcanic edifice. Numerical models on other shapes for magma systems are in progress and may allow a better understanding of the variations observed between volcanoes.

The stress analysis adopted here on a linear elastic, continuous, isotropic medium appears to be justified when modeling the structure of a whole edifice including the surrounding crust. It will not be the case if surface displacements or more local structural dynamics are to be analyzed. For instance, investigation of the mechanical behavior of a summit caldera, or the propagation of a fissure from the chamber to surface, or ground deformation, or the triggering of landslides, would require the use of a discontinuous elastoplastic model. The use of an anisotropic medium with temperature dependent elastic parameters must also be considered.

Analysis of the mechanical behavior of volcanoes needs to be coupled with rock mechanics like in situ stress measurements and determination of tensile strength of the rocks. Unfortunately, such data on volcanoes are sadly lacking. Geological investigations including petrology, geothermobarometry, seismology, and geophysics will also help to improve and constrain the mechanical modeling of volcanoes. This approach also offers an excellent opportunity for experimentation with scaled-down analog models.

Acknowledgements. This research was supported by the Department of Transport and the Department of Environment Affairs of the Republic of South Africa on a SASCAR program under the aegis of the Council for Scientific and Industrial Research. The part of the work dealing with Piton de la Fournaise volcano was done at the Observatoire Volcanologique de la Réunion under the aegis of the Institut de Physique du Globe de Paris. We gratefully acknowledge the Island Council of Tristan da Cunha for their sanctioning of research in the island and on Gough. We also wish to thank the Institute for Structural Engineering of the University of Stellenbosch for help and for the use of computing facilities.

References

Anderson, E. M., The dynamics of the formation of cone-sheets, ring dykes and cauldron subsidence, Proc. R. Soc. Edinburgh, 56, 128-157, 1935.

Bachélery, P., Le Piton de la Fournaise (Ile de la Réunion). Etude volcanologique, structurale et pétrologique, thèse de Donctorat de spécialité, 241 pp., Univ. de Clermont Ferrand, 1981.

Bachélery, P., and L. Chevallier, Carte volcano-tectonique du Piton de la Fournaise, scale 1/50,000, edited by Institut de Physique du Globe de Paris, Dir. des Observ. Volcanol. Fr. Univ. de Paris VI, 1982.

Bachélery, P., P. A. Blum, J. L. Cheminée, L. Chevallier, R. Gaulon, N. Girardin, C. Jaupart, F. X. Lalanne, J. L. LeMouel, J. C. Ruegg, and P. M. Vincent, Eruption at Le Piton de la Fournaise volcano on 3rd February 1981, Nature, 297, 395-397, 1982.

Baker, P. E., I. G. Gass, P. G. Harris, and R. W. LeMaitre, The volcanological report of the Royal Society Expedition to Tristan da Cunha, 1962, Philos. Trans. R. Soc., London, Ser. A, 256, 439-478, 1964.

Bianchi, R., A. Coradini, C. Federico, G. Giberti, G. Sartoris, and R. Scandone, Modeling of surface ground deformation in the Phlegrean Fields volcanic area, Italy, Bull. Volcanol., 47, 321-330, 1984.

Bonazia, V., F. Pingue, and R. Scarpa, A fluid-filled fracture as possible mechanism of ground deformation at Phlegrean Fields, Italy, Bull. Volcanol., 47, 313-320, 1984.

Carmichael, R. C. (Ed.), Handbook of Physical Properties of Rocks, vol. 2, CRC Press, Boca Raton, Fla., 1982.

Cheung, Y. K., and M. F. Yeo, A Practical Introduction to Finite Element Analysis, Pitman, London, 1979.

Chevallier, L., Tectonics of Marion and Prince Edward volcanoes (Indian Ocean): Result of regional control and edifice dynamics, Tectonophysics, 124, 155-175, 1986.

Chevallier, L., Tectonics and structural evolution of Gough volcano: A volcanological model, J. Volcanol. Geotherm. Res., 33, 325-336, 1987.

Chevallier, L., and P. Bachélery, Evolution structurale du volcan actif du Piton de la Fournaise, Ile de la Réunion, Océan Indien Occidental, Bull. Volcanol., 44(4), 723-741, 1981.

Chevallier, L., and N. Vatin Perignon, Volcano-structural evolution of Piton des Neiges on Réunion Island, Indian Ocean, Bull. Volcanol., 45(4), 285-298, 1982.

Chevallier, L., and W. J. Verwoerd, A dynamic interpretation of Tristan da Cunha volcano, South Atlantic Ocean, J. Volcanol. Geotherm. Res., 34, 35-50, 1987.

Chevallier, L., F. X. Lalanne, P. Bachélery, and P. M. Vincent, L'éruption du mois de Février 1981 au Piton de la Fournaise (Ile de la Réunion-Océan Indien), Phénomènologie et remarques structurales, C. R. Acad. Sci. Paris, 239, 187-190,1981.

Clark, S. P., Jr, Handbook of Physical constants, Mem. Geol. Soc. Am., 97, 587 pp., 1986.

Cloetingh, S., and R. Wortel, Regional stress field of the Indian Plate, Geophys. Res. Lett., 12, 77-80, 1985.

Davis, P. M., Surface deformation associated with a dipping hydrosurface, J. Geophys. Res., 88, 5826-5834, 1983.

Decker, R. W., Dynamics of Hawaiian volcanoes, an overview. Volcanism in Hawaii, vol. 2, edited by R. W. Decker, T. L. Wright and P. H. Stauffer, U.S. Geol. Surv. Prof. Pap., 1350, 997-1018, 1987.

Dieterich, J. H., and R. W. Decker, Finite element modeling of the surface deformation associated with volcanism, J. Geophys. Res., 80, 4094-4102, 1975.

Duffield, W. A., Structure and origin of the Koae fault system, Kilauea volcano, Hawaii, U.S. Geol. Surv. Prof. Pap., 856, 12 pp., 1975.

Eaton, J. P., Crustal structure and volcanism in Hawaii, in The Crust of the Pacific Basin, Geophys. Monogr. Ser. 6, edited by G. A. MacDonald and H. Kuno, pp. 13-29, AGU, Washington, D. C., 1962.

Fedotov, S. A., Ascent of basic magmas in the crust and mechanism of basaltic fissure eruptions, Int. Geol. Rev., 20, 33-48, 1976.

Feraud, G., G. Giannerini, R. Campredon, and C. J. Stillman, Geochronology of some Canarian dike swarms: Contribution to the volcano-tectonic evolution of the archipelago, J. Volcanol. Geotherm. Res., 25, 29-52, 1985.

Fiske, R. S., and W. T. Kinoshita, Inflation of Kilauea volcano prior to its 1967-1968 eruption, Science, 165, 341-349, 1969.

Gillot, P. Y., and P. Nativel, K/Ar chronology of the ultimate activity of Piton des Neiges volcano, Réunion Island, Indian Ocean, J. Volcanol. Geotherm. Res., 13, 131-146, 1982.

Giret, A., Le Plutonisme océanique intraplaque, Exemple de l'Archipel Kerguelen (TAAF), Thèse de Doctorat ès Sciences, 290 pp., Univ. P. et M. Curie, Paris VI, 1983.

Giret, A., and J. Lameyre, A study of Kerguelen plutonism: Petrology and geochronology, geological implications, in SCAR/IUGS Symposium on Antarctic Earth Sciences, edited by R. L. Oliver, P. R. James, and J. B. Jago, pp. 646-651, Cambridge University Press, New York, 1983.

Jackson, D. B., D. A. Swanson, R. Y. Koyanagi, and T. L. Wright, The August and October 1968 east rift eruptions of Kilauea volcano, Hawaii, U.S. Geol. Surv. Prof. Pap., 890, 33 pp, 1975.

Jeffreys, H., Note on fracture, Proc. R. Soc. Edinburgh, 56, 158-163, 1935.

Kieffer, G., B. Tricot, and P. M. Vincent, Une eruption inhabituelle (Avril 1977) du Piton de la Fournaise (Ile de la Réunion): ses enseignements volcanologiques et structuraux, C. R. Acad. Sci. Paris, 285, 957-960, 1977.

Klein, F. W., R. Y. Koyanagi, J. S. Nataka, and W. R. Tanigawa, The seismicity of Kilauea magma system, Volcanism in Hawaii, vol. 2. Edited by R. W. Decker, T. L. Wright and P. H. Stauffer, U.S. Geol. Surv. Prof. Pap., 1350, 1019-1186, 1987.

Krafft, M., and A. Gérente, L'activité du Piton de la Fournaise entre Octobre 1972 et Mai 1973 (Ile de la Réunion, Océan Indien), C. R. Acad. Sci. Paris, 284, 607-610, 1977a.

Krafft, M., and A. Gérente, L'activité du Piton de la Fournaise entre Novembre 1975 et Avril 1976 (Ile de la Réunion, Océan Indien), C. R. Acad. Sci. Paris, 284, 2091-2094, 1977b.

LeMaitre, R. W., The geology of Gough Island, South Atlantic, Overseas Geol. Min. Resour., 7, 371-380, 1960.

LeMaitre, R. W., Petrology of Volcanic rocks, Gough Island, South Atlantic, Bull. Geol. Soc. Am., 73, 1309-1340, 1962.

Lénat, J. F., P. Bacéhlery, A. Bonneville, P. Tarits, J. L. Cheminée, and H. Delorme, The December 4th February 1984 eruption of Piton de la Fournaise (La Réunion, Indian Ocean), Dynamism of magma transfers, J. Volcanol. Geotherm. Res., in press, 1988.

LeRoex, A. P., Geochemistry, mineralogy and magmatic evolution of the basaltic and trachytic lavas from Gough Island, South Atlantic, J. Petrol., 26, 149-186, 1985.

Lipman, P. W., The southwest rift zone of Mauna Loa: Implications for structural evolution of Hawaiian volcanoes, Am. J. Sci. 280, 752-776, 1980.

Lipman, P. W., J. P. Lockwood, R. T. Okamura, D. A. Swanson, and K. M. Yamashita, Ground deformation associated with the 1975 magnitude-7.2 earthquake and resulting changes in activity of Kilauea volcano, Hawaii, U.S. Geol. Surv. Prof. Pap., 1276, 45 pp., 1985.

Ludden, J. N., Magmatic evolution of the basaltic shield volcanoes of Réunion Island, J. Volcanol. Geotherm. Res., 4, 171-198, 1978.

McDougall, I., Geochronology, in Marion and Prince Edward Islands, edited by E. M. van Zinderen Bakker, J. M. Winterbottom, and R. A. Dyer, pp. 72-77, A. A. Balkema, Cape Town, 1971a.

McDougall, I., The geochronology and evolution of the young volcanic island of Réunion, Indian Ocean, Geochim. Cosmochim. Acta, 35 , 261-288, 1971b.

McDougall, I., and C. Ollier, Potassium argon ages from Tristan da Cunha, South Atlantic, Geol. Mag., 119, 87-93, 1982.

Mogi, K., Relations between the eruptions of various volcanoes and the deformation of the ground surface around them, Bull. Earthquake Res. Inst. 36, 99-135, 1958.

Muller, O. H., Changing stresses during emplacement of the radial dyke swarm of Spanish Peaks, Colorado, Geology, 14, 157-159, 1986.

Nakamura, K., Volcanoes as possible indicators of tectonic stress orientation: Principle and proposal, J. Volcanol. Geotherm. Res., 2, 1-16, 1977.

Ollier, C. D., Geomorphology of South Atlantic volcanic islands, I, The Tristan da Cunha Group, Z. Geomorphol. 28, 367-382, 1984.

Paquin, C., J. Bloyet, and C. Angelidis, Tectonic stresses on the boundary of the Aegean domain: "In situ" measurements by overcoring, Tectonophysics, 110, 145-150, 1984.

Paul, A., J. P. Gratier, and J. A. Boudon, A numerical model for simulating deformation of Mount St. Helens volcano, J. Geophys. Res., 92, 10,299-10,312, 1987.

Phillips, W. J., The dynamics of emplacement of cone sheets, Tectonophysics, 24, 69-84, 1974.

Pollard, D. D., Equations for stress and displacement fields around pressurized elliptical holes in elastic solids, Math. Geol., 5, 11-25, 1973a.

Pollard, D. D., Derivation and evaluation of a mechanical model for sheet intrusions, Tectonophysics, 19, 233-269, 1973b.

Pollard, D. D., and G. Holzhausen, On the mechanical interaction between a fluid-filled fracture and the earth's surface, Tectonophysics, 53, 27-57, 1969.

Pollard, D. D., P. T. Delaney, W. A. Duffield, E. T. Endo, and A. T. Okamura, Surface deformation in volcanic rift zones, Tectonophysics, 94, 541-584, 1983.

Robson, G. R., and K. G. Barr, The effect of stress on faulting and minor intrusions in the vicinity of a magma body, Bull. Volcanol., 27, 315-350, 1964.

Roobol, M. J., The geology of the Vesturhorn intrusion, SE Iceland, Geol. Mag., 111(4), 273-285, 1974.

Ryan, M. P., Elasticity and contractancy of Hawaiian olivine tholeiite and its role in the stability and structural evolution of subcaldera magma reservoirs and rift systems. Volcanism in Hawaii, vol. 2, Edited by R. W. Decker, T. L. Wright and P. H. Stauffer, U.S. Geol. Surv. Prof. Pap., 1350, 1395-1447, 1987a.

Ryan, M. P., Neutral buoyancy and the mechanical evolution of magmatic systems, in Magmatic Processes: Physicochemical Principles, Spec. Publ. 1, edited by B. O. Mysen, pp. 259-287, The Geochemical Society, Ann Arbor, Mich. 1987b.

Ryan, M. P., J. Y. K. Blevins, A. T. Okamura, and R. Y. Koyanagi, Magma reservoir subsidence mechanics: Theoretical summary and application to Kilauea volcano, Hawaii, J. Geophys. Res., 88, 4147-4183, 1983.

Swanson, D. A., W. A. Duffield, and R. S. Fiske, Displacement of the South Flank of Kilauea volcano: The result of forceful intrusion of magma into the rift zones, U.S. Geol. Surv. Prof. Pap., 963, 1-139, 1976.

Tryggvason, E., Multiple magma reservoirs in a rift zone volcano: Ground deformation and magma transport during the September 1984 eruption of Krafla, Iceland, J. Volcanol. Geotherm. Res., 28, 1-44, 1986.

Tsunakawa, H., Simple two-dimensional model of propagation of magma-filled cracks, J. Volcanol. Geotherm. Res., 16, 335-343, 1983.

Upton, B. G. J., and W. J. Wadsworth, Aspects of magmatic evolution on Réunion Island, Philos. Trans. R. Soc. London, Ser. A, 271, 105-130, 1972.

Verwoerd, W. J., Geology, in Marion and Prince Edward Islands, edited by E. M. van Zinderen Bakker, J. M. Winterbottom, and R. A. Dyer, pp. 40-62, A. A. Balkema, Cape Town, 1971.

Verwoerd, W. J., and L. Chevallier, Contrasting types of Surtseyan tuff cones on Marion and Prince Edward islands, South West Indian Ocean, Bull. Volcanol., 49, 399-417, 1987.

Verwoerd, W. J., S. Russell, and A. Berruti, 1980 volcanic eruption reported on Marion Island, Earth Planet. Sci. Lett., 54, 153-156, 1981.

Walsh, J. B., and R. W. Decker, Surface deformation associated with volcanism, J. Geophys. Res., 76, 3291-3308, 1971.

Wood, C. A., Morphometric evolution of cinder cones, J. Volcanol. Geotherm. Res., 7, 387-413, 1980.

Yokoyama, I., A model for the crustal deformations around volcanoes, J. Phys. Earth, 19, 199-207, 1971.

L. Chevallier and W. J. Verwoerd, Department of Geology, University of Stellenbosch, Stellenbosch 7600, South Africa.

(Received February 6, 1987;
revised June 25, 1987;
accepted November 6, 1987)